INTERNATIONAL JOURNAL FOR NUMERICAL METHODS IN FLUIDS, VOL. 14, 1219–1243 (1992)

TWO-DIMENSIONAL WAVE RUN-UP ANALYSIS BY SELECTIVE LUMPING FINITE ELEMENT METHOD

TAKASHI OKAMOTO

Steel Research Center, Nippon Kokan K. K., 1-1, Minamiwatarida-cho, Kawasaki-ku, Kawasaki, Japan

MUTSUTO KAWAHARA AND NOBUHIRO IOKI

Department of Civil Engineering, Chuo University, Kasuga 1-Chome 13, Bunkyo-ku, Tokyo, Japan

AND

HIROAKI NAGAOKA

Steel Research Center, Nippon Kokan K.K., 1-1, Minamiwatarida-cho, Kawasaki-ku, Kawasaki, Japan

SUMMARY

A new finite element technique for the analysis of wave run-up is presented in this paper. In this finite element approach, the movement of the shoreline is expressed by that of the nodal points at the wave front, and an auto mesh generation technique is effectively used. The present method is tested by the comparison with the experimental result of a channel with uniform slope, and two numerical examples are reported to show the efficiency of this method. As a final example, the tsunami run-up caused by the 1983 Nihonkai-Chubu earthquake is analysed and compared with actual records of the flooded area.

1. INTRODUCTION

Wave run-up along a coast is an interesting and important engineering problem. For example, consider a tsunami. When the tsunami arrives at the coastline, the run-up of the tsunami wave towards the land causes tremendous damage to man-made structures. Therefore it is essential to be able to predict how far a tsunami will run up over the land area. There have been numerous analyses of this problem. Experimental studies were carried out by Ippen and Kulin,[1] Kaplan,[2] Kishi,[3] Iwagaki *et al.*,[4] Iwagaki,[5] Camfield and Street,[6] Nakamura and Togashi[7,8] and Togashi and Nakamura,[9] who proposed predictive equations based on their experimental results. Carrier and Greenspan,[10] Greenspan,[11] Shuto and Matsumura,[12] Shuto[13,14] and Grimshaw[15] gave theoretical solutions to a limited extent. Most numerical studies were carried out by the method of characteristics or the finite difference method (see e.g. References 16–24). Finite element studies were done by Heitner and Housner[25] and Gopalakrishnan and Tung.[26,27] However, most of the above studies were restricted to one-dimensional analysis because of the complicated characteristics of the problem.

This paper presents a two-dimensional numerical analysis of wave run-up by the finite element method. In the analysis of wave run-up the finite element method is one of the most effective analytical tools because the complex geometry of a land boundary can be handled easily. However, the difficulty that arises in the application to wave run-up is the fact that the boundary will move. To pursue a moving boundary, a complicated algorithm must be introduced. This

0271–2091/92/101219–25$12.50

Received May 1988
Revised September 1991

paper presents a new finite element technique for the analysis of wave run-up. In this technique the movement of the shoreline is expressed by the movement of the nodal points at the wave front and the region where fluid exists always agrees with the region to be analysed. To express the movement, an automatic mesh generation technique is introduced and used effectively. With this method one can handle the moving boundary problem in a relatively easy manner.

To examine the validity of the method, one-dimensional experiments on a channel with uniform slope are analysed and comparisons are made between the calculated and experimental results. Good agreement is found, showing that reasonable results can be obtained with the present rmethod. After several test examinations, two examples are analysed, namely one-dimensional wave run-up in a channel of non-uniform slope (composite slope) and two-dimensional run-up in a channel of wedge-shaped cross-section. Reasonable calculated results are obtained, showing that the present method is adaptable for the analysis of complex problems. As a final numerical example, the tsunami run-up caused by the 1983 Nihonkai-Chubu earthquake is analysed and compared with the actual records of the flooded area.

2. FINITE ELEMENT EQUATION

According to shallow water wave theory, the basic equations of wave run-up are the equation of motion,

$$\dot{U}_i + U_j U_{i,j} + g\eta_{,i} + f(U\cos\alpha)_i = 0, \tag{1}$$

and the equation of continuity,

$$\dot{\eta} + [U_i(h+\eta)]_{,i} = 0, \tag{2}$$

where U_i is the mean velocity in the direction of the x_i-co-ordinate, η, h and g are the water elevation relative to the still water level, the depth of water and the gravitational acceleration respectively, f is the coefficient of bottom friction and α is the angle of beach slope.

The standard Galerkin finite element method is applied to equations (1) and (2) for spatial discretization and the selective lumping two-step explicit finite element method is employed for numerical integration in time. For the interpolation functions of velocity and water elevation, standard linear functions based on the three-node triangular finite element are used. Let $U_{\beta i}$ and η_β be the velocity in direction x_i and the water elevation at node β respectively. The following numerical integration procedure can be derived:[28-32]

for the first step,

$$\tilde{M}_{\alpha\beta} U^{n+1/2}_{\beta i} = \tilde{M}_{\alpha\beta} U^n_{\beta i} - (\Delta t/2)[K_{\alpha\beta\gamma,j} U^n_{\beta j} U^n_{\gamma i} + gN_{\alpha\beta,i}\eta^n_\beta + fM_{\alpha\beta}(U\cos\alpha)^n_{\beta i}], \tag{3}$$

$$\tilde{M}_{\alpha\beta}\eta^{n+1/2}_\beta = \tilde{M}_{\alpha\beta}\eta^n_\beta - (\Delta t/2)\{K_{\alpha\beta\gamma,i}[U^n_{\gamma i}(h_\beta + \eta^n_\beta) + U^n_{\beta i}(h_\gamma + \eta^n_\gamma)]\}; \tag{4}$$

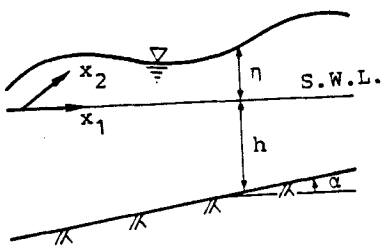

Figure 1. Co-ordinate system

for the second step,

$$\bar{M}_{\alpha\beta}U_{\beta i}^{n+1}=\tilde{M}_{\alpha\beta}U_{\beta i}^{n+1/2}-\Delta t[K_{\alpha\beta\gamma,j}U_{\beta j}^{n+1/2}U_{\gamma i}^{n+1/2}+gN_{\alpha\beta,i}\eta_{\beta}^{n+1/2}+fM_{\alpha\beta}(U\cos\alpha)_{\beta i}^{n+1/2}], \quad (5)$$

$$\bar{M}_{\alpha\beta}\eta_{\beta}^{n+1}=\tilde{M}_{\alpha\beta}\eta_{\beta}^{n+1/2}-\Delta t\{K_{\alpha\beta\gamma,i}[U_{\gamma i}^{n+1/2}(h_{\beta}+\eta_{\beta}^{n+1/2})+U_{\beta i}^{n+1/2}(h_{\gamma}+\eta_{\gamma}^{n+1/2})]\}. \quad (6)$$

Superscript n denotes the value at the nth time step. $M_{\alpha\beta}$, $K_{\alpha\beta\gamma}$ and $N_{\alpha\beta}$ are coefficients obtained from the discretization procedure by the finite element method. $\bar{M}_{\alpha\beta}$ expresses the lumped coefficient and $\tilde{M}_{\alpha\beta}$ is the selective lumping coefficient, i.e.

$$\tilde{M}_{\alpha\beta}=e\bar{M}_{\alpha\beta}+(1-e)M_{\alpha\beta}, \quad (7)$$

where e is the selective lumping parameter. The parameter usually takes a value about $e=0{\cdot}8$–$0{\cdot}95$ and the value of $0{\cdot}9$ is employed in the present paper.

Using the selective lumping technique, which combines both lumped and unlumped coefficients, a stable computation can be obtained and minimization of the error due to artificial damping can be realized.[28–32]

3. CALCULATION OF MOVING SHORELINE

The initial finite element idealization is carried out at the still water level. The movement of the shoreline is expressed by the movement of the nodal points at the wave front and the region where fluid exists always agrees with the region to be analysed. According to this method, since the moving boundary is always the wave front at each time step, the explicit two-step scheme, i.e. the calculation of equations (3)–(6), can be applied.

The method by which a nodal point moves is explained as follows. As shown in Figure 2, the shoreline moves a horizontal distance S in the time interval Δt. Using the velocity and acceleration of the water at the wave front, the next position of the nodal point can be calculated.

The mean acceleration a_i^{m} of each nodal point at the wave front in the period between t and $t+\Delta t$ is described in the following manner. The average of the accelerations a^t and $a^{t+\Delta t}$ at times t and $t+\Delta t$ is calculated as

$$a_i^{\mathrm{m}}=\tfrac{1}{2}(a_i^t+a_i^{t+\Delta t}). \quad (8)$$

The Lagrangian acceleration of a nodal point at time t is computed as

$$a_i=\dot{U}_i^f+U_j^f U_{i,j}^f, \quad (9)$$

where a_i denotes the acceleration of nodal point i in direction x_i and U_i^f is the Eulerian velocity of the water at the wave front. From equations (8) and (9) the movement distance S_i in direction x_i can be calculated as

$$S_i=U_i^{\mathrm{c}}\Delta t+\tfrac{1}{2}a_i^{\mathrm{m}}(\Delta t)^2. \quad (10)$$

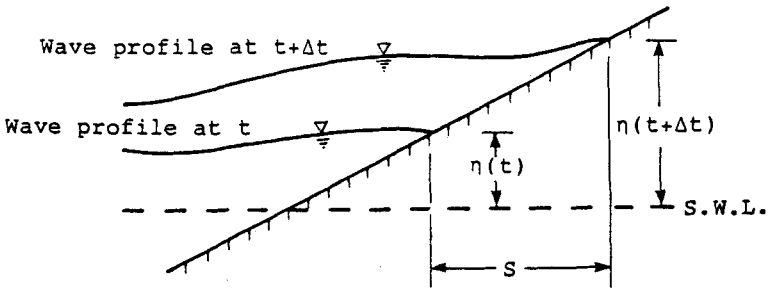

Figure 2. Wave profiles at t and $t+\Delta t$

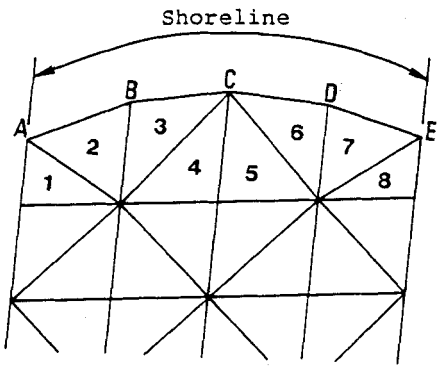

Figure 3. Elements in contact with a shoreline

In the calculation of the second term on the right-hand side of equation (8) the gradient of U_i is constant in each finite element because the interpolation function of velocity U_i is linear. The gradient of U_i at nodal points in contact with the shoreline can be calculated as the average value over the elements around the nodal point as

$$[U_{i,j}]_N=(1/K)\sum_{L=1}^{K}[U_{i,j}]_{E(L)}, \tag{11}$$

where N is the node number, $E(L)$ is the number of the Lth element which contacts node N and K is the total number of elements connecting with node N.

In the case shown in Figure 3 the velocity gradient can be calculated in the following manner. Nodes from A to E are the nodal points which contact the shoreline. Point C is taken up as an example. Nodal point C is connected with the elements numbered 3, 4, 5 and 6. The velocity gradient of nodal point C is calculated by dividing the total sum of the velocity gradients of elements 3, 4, 5 and 6 by four, which is the total number of elements which connect with nodal point C.

4. AUTOMATIC MESH GENERATION TECHNIQUE

There is a computational advantage in this method that the movement of the shoreline is expressed by the movement of the nodal points at the wave front. On the other hand, there is a disadvantage that the area of the finite elements which contact the shoreline varies with time. If the wave moves upwards to the beach, the nodal points on the shoreline must move upwards and the size of elements increases. Conversely, if the wave moves downwards, the size of elements decreases. In an ordinary finite element analysis, elements which are too large or too small cause numerical instability and inaccurate computation.

In order to overcome these difficulties, regeneration of the finite elements is carried out by an automatic mesh generation technique which is newly developed in this paper, i.e. if the size of an element becomes larger than the standard, the element is divided into two elements, and if the size of an element becomes smaller than the standard, the element is eliminated from the computational domain. By this technique the finite element idealization adapts the domain to be analysed and the size of elements can be kept constant as far as possible. The following is an explanation of the automatic mesh generation technique.

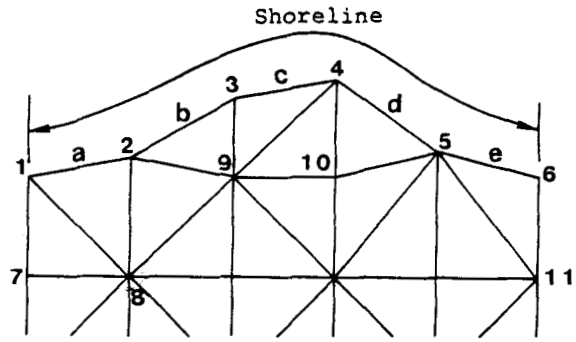

Figure 4. Example of mesh auto-generation technique

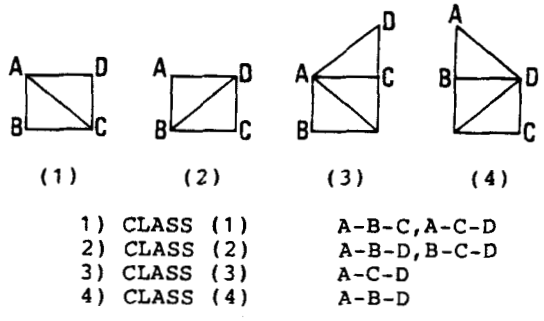

Figure 5. Classification of elements

Table I. Example of classification of elements

Element column	Class
a	1
b	3
c	2
d	4
e	1

4.1. Determination of the moving boundary

The mesh shown in Figure 4 is used as an example to explain the automatic mesh generation technique. Nodes numbered from 1 to 6 are the nodes which contact the shoreline. As shown in Figure 5, the elements which contact the shoreline are classified into four classes based on the manner of connection of nodal points to the nearest shoreline. The automatic mesh generation can be effectively applied after this classification.

In Figure 5, side A–D expresses the shoreline and nodal points A and D are moved on the basis of equation (10). The case shown in Figure 4 is classified as in Table I.

4.2. Generation of elements

In the case of a wave moving upwards as shown in Figure 6, the lengths of sides A–B and D–C extend. If either side A–B or D–C has a length L which is larger than the standard length L_s, the

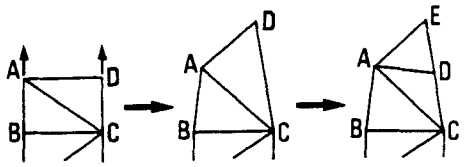

Figure 6. Generation of an element

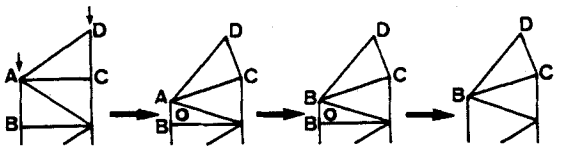

Figure 7. Elimination of an element

element is split into two elements and the size is kept as constant as possible. Figure 6 is the case of CLASS (1). The length L of D–C is larger than the standard length L_s and the element is split into two elements ACD and ADE.

4.3. Elimination of elements

In the case of a wave moving downwards as shown in Figure 7, the lengths of sides A–B and D–C are shortened. If either side A–B or D–C has a length L which is smaller than half the standard length L_s, the element is eliminated. Figure 7 is the case of CLASS (3). The length L of A–B is smaller than half the standard length L_s and the element marked 'o' is eliminated.

Figures 6 and 7 are two examples of automatic mesh generation. All possible cases of automatic mesh generation appearing in calculations are shown in Figure 8, where parameters a and b in CASE (a, b) have the following meaning.

$a=0$: $\frac{1}{2}L_s<\mathrm{AB}<2L_s$,

$a=1$: $\mathrm{AB}\geqslant 2L_s$,

$a=2$: $\mathrm{AB}\leqslant\frac{1}{2}L_s$,

$b=0$: $\frac{1}{2}L_s<\mathrm{CD}<2L_s$,

$b=1$: $\mathrm{CD}\geqslant 2L_s$,

$b=2$: $\mathrm{CD}\leqslant\frac{1}{2}L_s$,

where AB and CD are the lengths of sides A–B and C–D respectively.

4.4. Interpolation of water depth

The nodal points at the shoreline are moved according to the movement of fluid. It is necessary to correct the data of depth for the moved nodal points at each time step.[35]

Assume that the shoreline has moved as shown in Figure 9, where the line from A to E is the shoreline. Solid lines represent the finite element idealization used for the computation of fluid and dotted lines that used for the interpolation of water depth. If nodal point C is located on

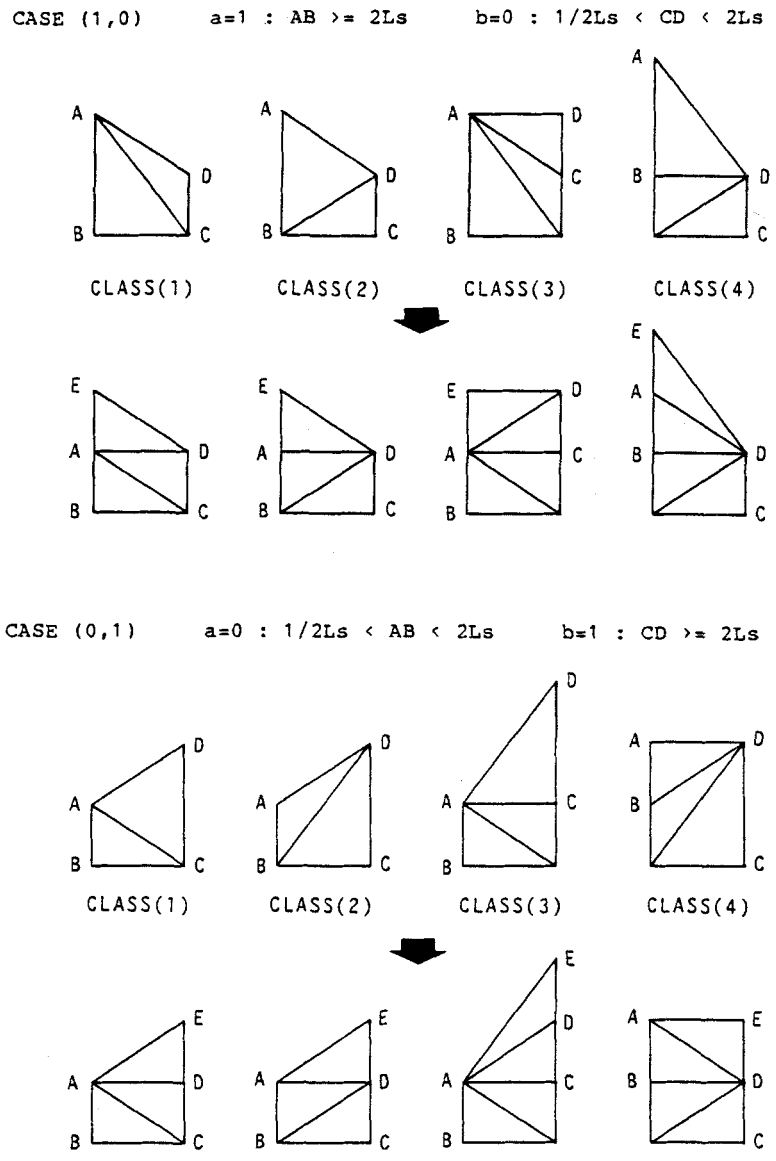

Figure 8(a). Mesh auto-generation pattern

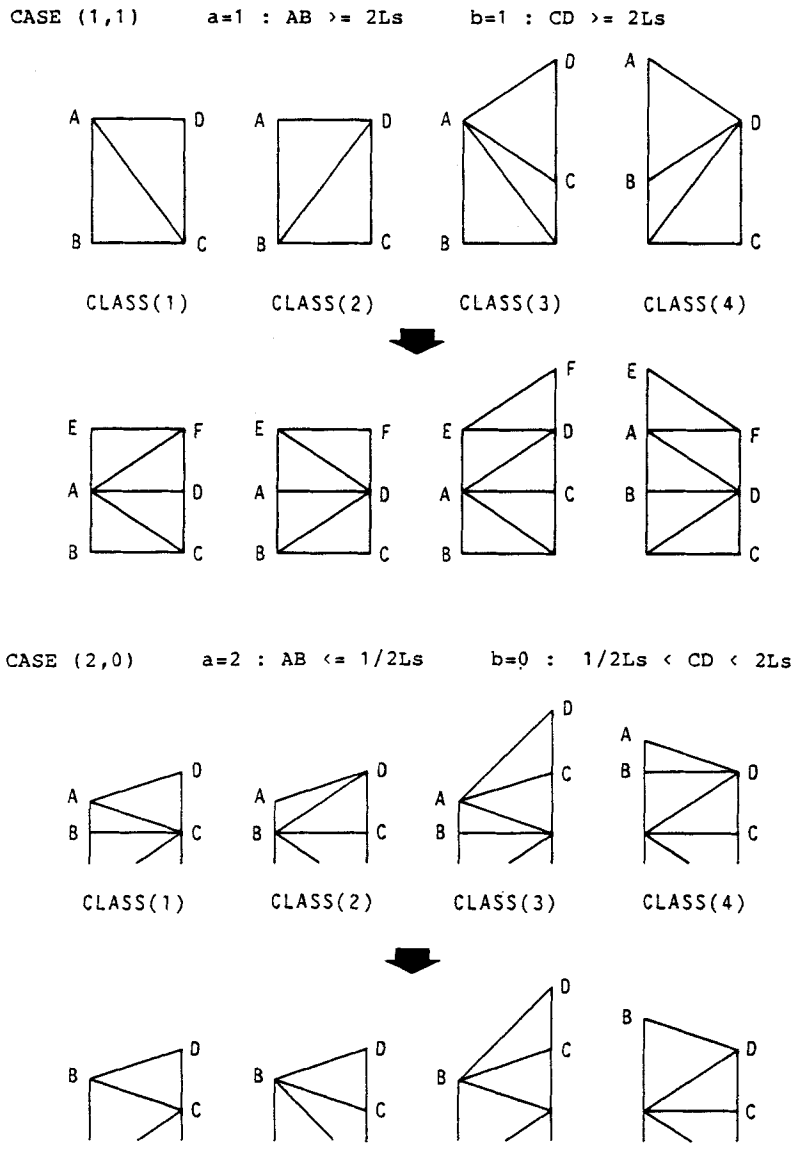

Figure 8(b). Mesh auto-generation pattern

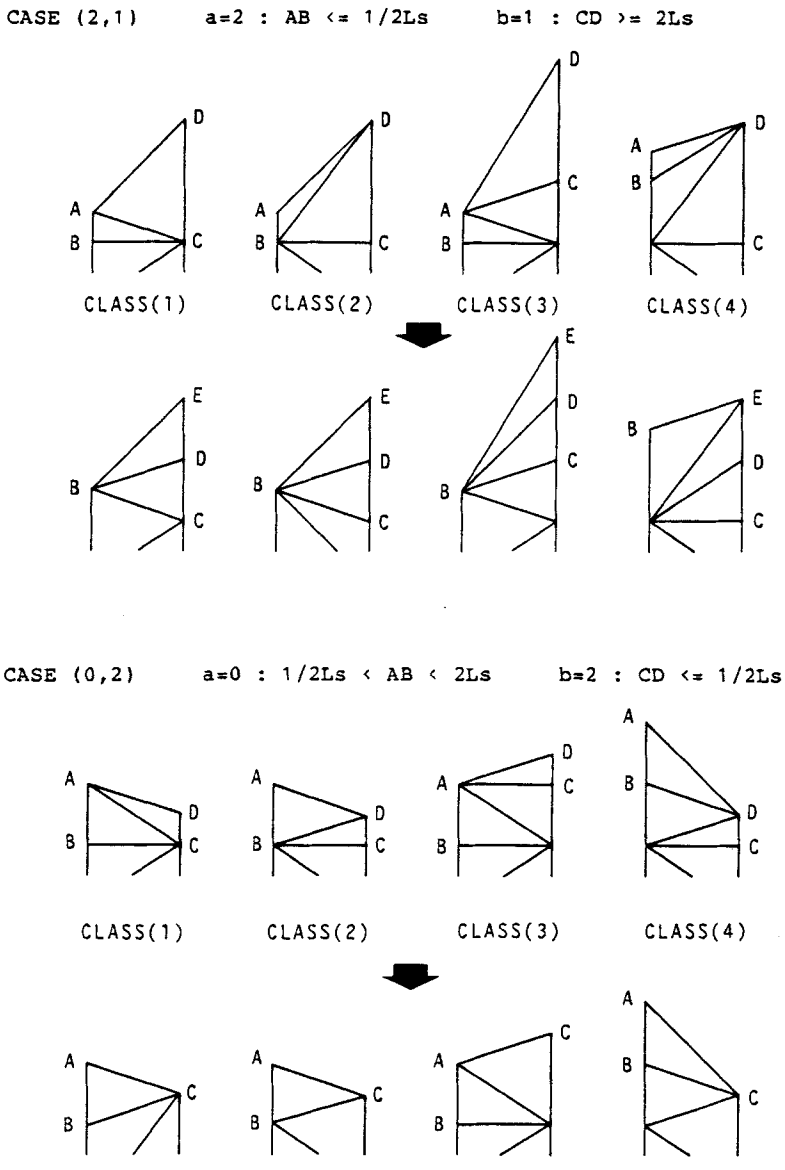

Figure 8(c). Mesh auto-generation pattern

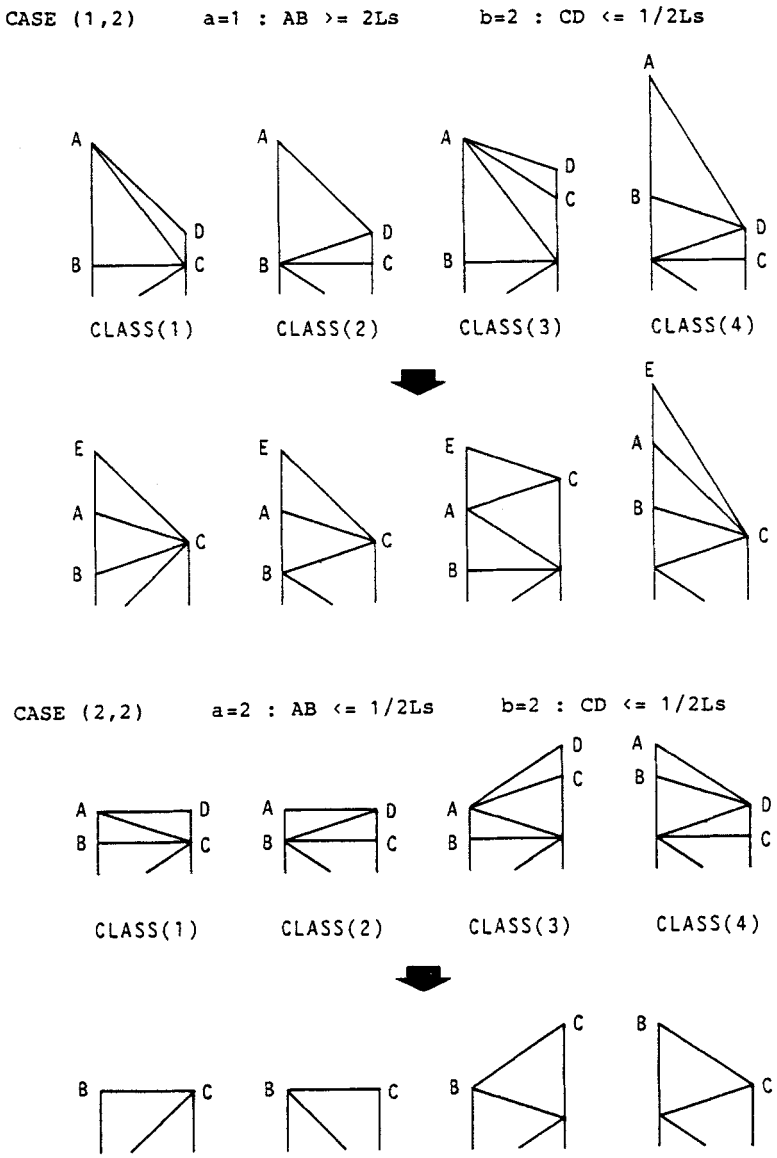

Figure 8(d). Mesh auto-generation pattern

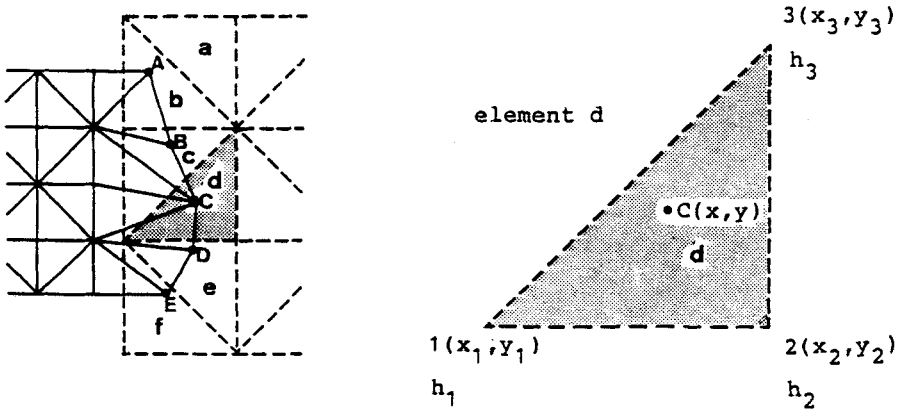

——— Finite element idealization used in computation
------ Finite element idealization used in interpolation of water depth
A - E Nodal points on the shoreline
a - f Element number

Figure 9. Interpolation of water depth

element d, then element d is the finite element which is used for the interpolation of water depth at C. The depth of nodal point C is corrected by the interpolation function of element d as

$$h_c = \Phi_1(x, y)h_1 + \Phi_2(x, y)h_2 + \Phi_3(x, y)h_3, \tag{12}$$

where Φ_i is the linear interpolation function and h_i is the depth of each nodal point of element d. The water depth h_c is the corrected depth of nodal point C.

5. NUMERICAL EXAMPLES

5.1. Comparison with experimental results

To investigate the validity of the method presented in this paper, a comparison with experimental results[13] has been carried out. The experiments were performed in a long wave channel of uniform slope connected with a horizontal bed (channel length 150 m, including length of beach slope, 25 m; width 6 m; depth 1 m). Experimental waves were generated by a pneumatic-type wave generator located at the end of the channel. The beach slope is $\tan\alpha = 1/30$. Experiments were carried out changing the water depth, the wave amplitude and the wave period.

The computational model is shown in Figure 10(a). Figure 10(b) is the finite element idealization in the still water state, where the lengths of finite elements are 1·05 m with $h = 35$ cm, 1·5 m with $h = 30$ cm and 1·5 m with $h = 25$ cm. Fifty cases of calculation were carried out as shown in Table II.

The boundary conditions used are as follows:

$$v = 0 \quad \text{on a–d and b–c,}$$

$$\eta = A\sin(2\pi/T)t \quad \text{on a–b,} \tag{13a}$$

$$u = \eta\sqrt{[(g/(h+\eta)]} \quad \text{on a–b,} \tag{13b}$$

Table II. Wave conditions and comparison of calculated and experimental results

	Wave conditions			Experimental results			Calculated results		
Case	h(cm)	$T/2$(s)	A(cm)	H'(cm)	R(cm)	R/H'	H'(cm)	R(cm)	R/H'
1	30	120	6·0	13·0	13·9	1·07	12·0	12·4	1·03
2	30	160	5·3	12·7	11·6	0·91	10·7	10·8	1·01
3	30	40	7·5	10·0	20·0	2·00	12·1	21·0	1·74
4	30	60	10·3	16·3	26·0	1·60	20·4	29·7	1·46
5	30	75	10·0	15·9	20·1	1·26	20·7	26·1	1·26
6	30	70	9·0	15·0	21·1	1·41	18·5	23·5	1·27
7	30	75	8·7	16·5	18·7	1·13	17·9	21·8	1·22
8	30	80	9·0	17·5	24·0	1·37	18·7	22·0	1·18
9	30	60	6·7	11·0	15·0	1·36	13·1	17·2	1·31
10	30	75	7·0	11·6	16·4	1·41	14·2	16·6	1·17
11	30	60	5·6	10·0	14·5	1·45	10·9	13·8	1·27
12	30	160	8·2	15·0	17·4	1·16	16·7	16·9	1·01
13	30	120	6·0	12·0	13·2	1·10	12·0	12·4	1·03
14	30	180	8·7	16·0	17·5	1·09	17·7	18·0	1·02
15	25	50	7·0	14·0	16·8	1·20	12·9	18·8	1·46
16	25	60	6·0	9·8	14·5	1·48	11·8	15·0	1·27
17	25	45	5·9	9·5	15·4	1·62	10·4	15·3	1·47
18	25	60	6·0	10·4	14·9	1·43	11·8	15·0	1·27
19	25	80	7·9	14·1	17·8	1·26	16·5	19·2	1·16
20	25	60	5·7	11·0	13·3	1·21	11·2	14·1	1·26
21	25	80	7·0	12·0	15·2	1·27	14·4	16·5	1·15
22	25	100	7·5	12·9	15·5	1·20	15·4	16·0	1·04
23	25	70	5·1	8·7	12·1	1·39	10·2	11·7	1·15
24	25	160	8·8	16·0	17·5	1·09	18·0	18·2	1·01
25	25	115	8·1	16·0	16·5	1·03	16·3	16·8	1·03
26	25	120	5·7	11·1	13·3	1·20	11·4	11·8	1·04
27	35	55	9·6	18·0	24·6	1·37	20·1	31·0	1·54
28	35	60	7·0	15·6	18·7	1·20	13·6	19·3	1·42
29	35	80	9·0	19·0	21·5	1·13	17·8	22·1	1·24
30	35	65	6·3	11·5	14·4	1·25	12·9	16·4	1·27
31	35	80	7·6	16·0	17·2	1·08	15·1	17·5	1·16
32	35	120	9·0	18·5	20·5	1·11	16·7	17·5	1·05
33	35	80	4·7	10·8	13·0	1·20	9·2	9·7	1·05
34	35	120	6·0	13·5	14·0	1·04	11·5	11·9	1·04
35	30	120	8·5	18·5	17·3	0·94	17·1	17·7	1·04
36	30	120	7·1	15·4	14·4	0·94	14·2	14·7	1·04
37	30	110	6·0	13·0	17·3	1·33	11·9	12·4	1·04
38	30	160	8·6	18·9	20·6	1·09	17·5	17·8	1·02
39	30	160	7·0	15·4	18·4	1·20	14·2	14·4	1·01
40	30	120	9·3	19·1	19·5	1·02	18·7	19·4	1·04
41	30	180	8·6	18·4	18·9	1·03	17·5	17·8	1·02
42	30	120	8·7	17·9	18·9	1·06	17·5	18·2	1·04
43	30	180	5·6	12·0	13·0	1·08	11·3	11·4	1·01
44	25	150	9·8	20·8	21·8	1·05	20·1	20·4	1·02
45	25	180	5·8	12·5	10·3	0·82	11·8	11·9	1·01
46	25	140	11·5	25·2	22·5	0·89	23·6	24·3	1·03
47	25	120	9·0	19·6	18·7	0·95	18·2	18·8	1·03
48	25	120	8·6	18·7	20·8	1·11	17·3	18·0	1·04
49	25	120	8·7	19·0	20·5	1·08	17·5	18·2	1·04
50	35	160	9·3	20·3	20·1	0·99	17·3	17·6	1·02

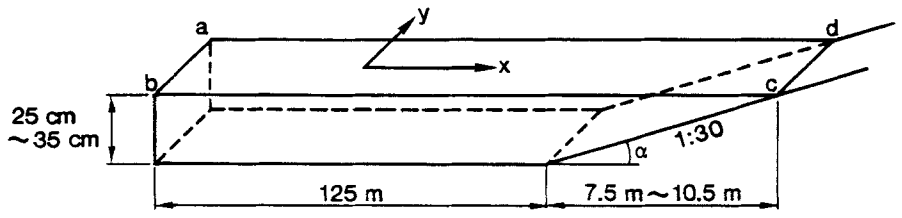

(a) Computational model

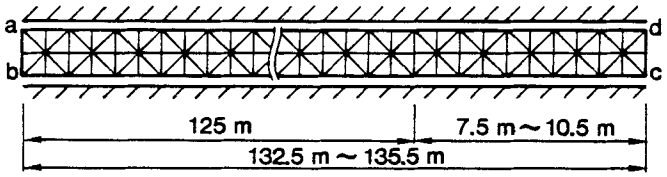

(b) Finite element idealization

Figure 10. Computational model and finite element idealization

where u and v are the velocities in directions x and y respectively, A is the amplitude (half-wave height) of sinusoidal forced oscillation, T is the wave period, η is the water elevation and g is the gravitational acceleration. Equations (13) correspond to the progressive wave condition. The initial conditions of velocity and water elevation are assumed to be zero for all domains analysed. A selective lumping parameter $e=0{\cdot}9$ and a time increment $\Delta t=0{\cdot}05$ s are employed.

The experimental and calculated results are shown in Table II. R is the run-up height and H' is the maximum water elevation at the edge of the slope as shown in Figure 11. Figures 12 and 13 show the comparison of experimental and calculated results for H' and R respectively. Open circles represent the computed results, which are close to the experimental results shown by the solid line. Four examples of the wave-form calculated by this method are shown in Figures 14 and 15. Figure 14 shows two cases based on the same wave periods and water depths but different amplitudes. Figure 15 shows two cases based on the same wave amplitudes and water depths but different wave periods.

In order to examine numerically the influence of forced oscillation amplitude, further calculations have been carried out. Figure 16 shows the calculated relationship between R/H' and l/L, where L is the wavelength ($L=\sqrt{(gh)}T$, where T is the period of forced oscillation) and l is the horizontal length of the slope as shown in Figure 11 in which the amplitude (half-wave height) of forced oscillation is changed from $A=2{\cdot}5$ to $15{\cdot}0$ cm. The water depth is 30 cm. Six examples of the wave-form calculated by this method are shown in Figures 17 and 18. Figure 17 shows three cases where the wave period is 60 s and the amplitude varies between $2{\cdot}5$ and $15{\cdot}0$ cm. Figure 18 shows three cases where the wave period is 130 s and the amplitude varies between $2{\cdot}5$ and $15{\cdot}0$ cm.

5.2. Run-up analysis of non-uniform slope

As an example of the analysis of a non-uniform slope beach, a run-up analysis of a composite slope beach is carried out. Figure 19(a) shows the computational model used for the analysis. The beach slopes are $\tan\alpha_1=1/30$, $\tan\alpha_2=0$ and $\tan\alpha_3=1/60$ and the slope lengths are $l_1=12$ m and

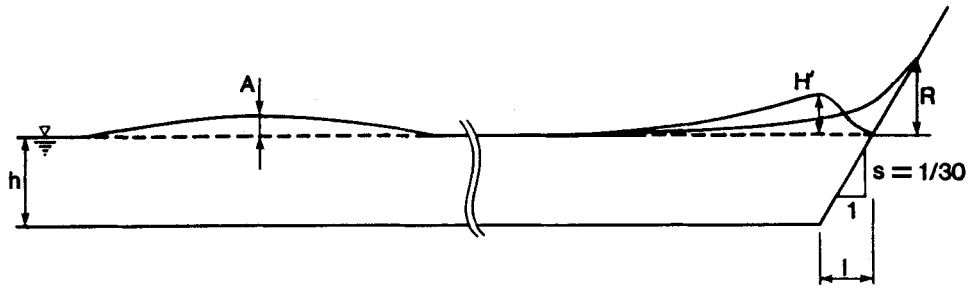

Figure 11. Explanation of symbols

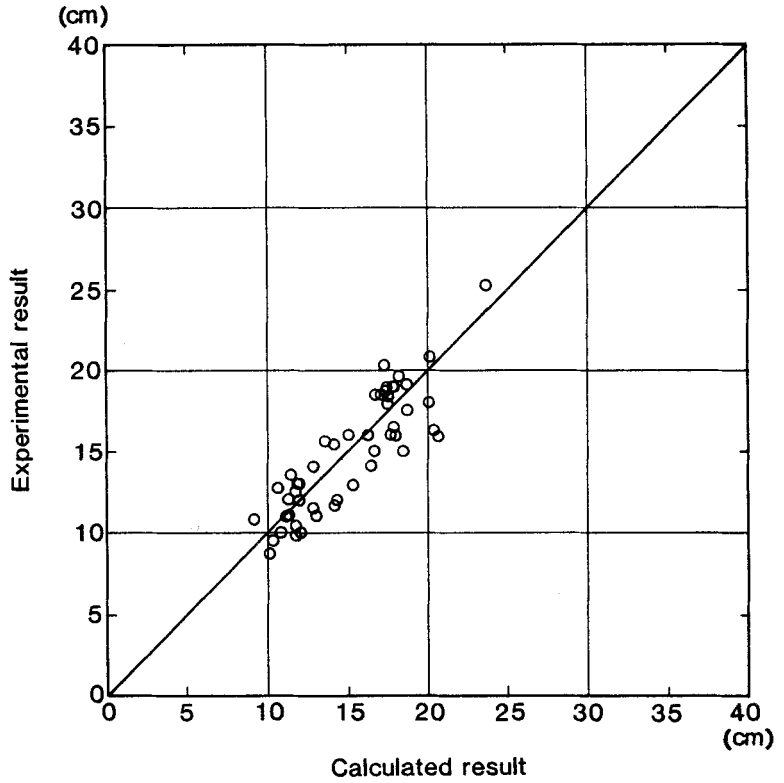

Figure 12. Comparison between computed and experimental results for H'

$l_2 = 6$ m. The water depth h is 30 cm. At the entrance to the channel a–b, sinusoidal forced oscillation is imposed. The amplitude A (half-wave height) is 10 cm and the wave period T is 100 s. Figure 19(b) is the finite element idealization in the still water state, where the lengths of finite elements are 1·5 m.

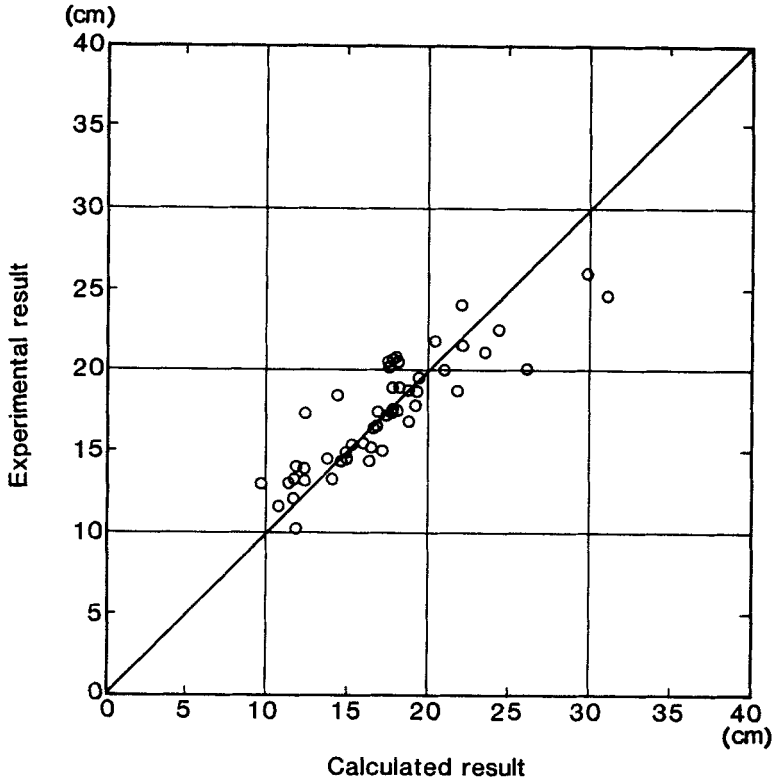

Figure 13. Comparison between computed and experimental results for R

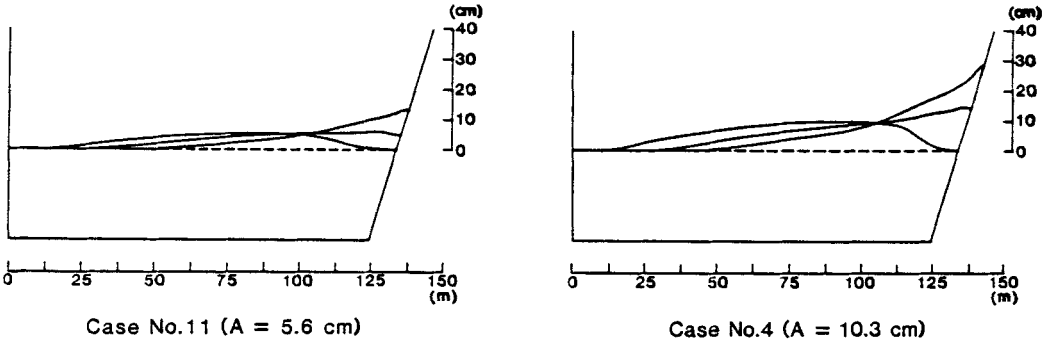

Figure 14. Wave profiles for cases 11 and 4

The boundary conditions used are as follows:

$$v=0 \quad \text{on a–d and b–c,}$$

$$\eta=A\sin(2\pi/T)t \qquad \text{on a–b,} \tag{14a}$$

$$u=\eta\sqrt{[g/(h+\eta)]} \qquad \text{on a–b.} \tag{14b}$$

Equations (14) correspond to the progressive wave condition.

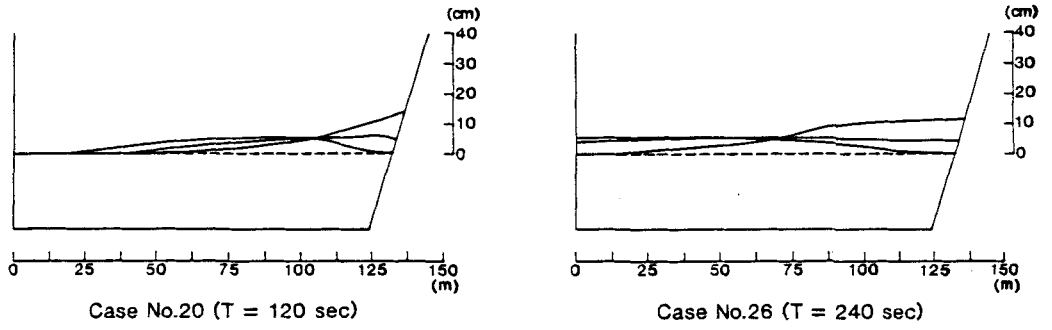

Figure 15. Wave profiles for cases 20 and 26

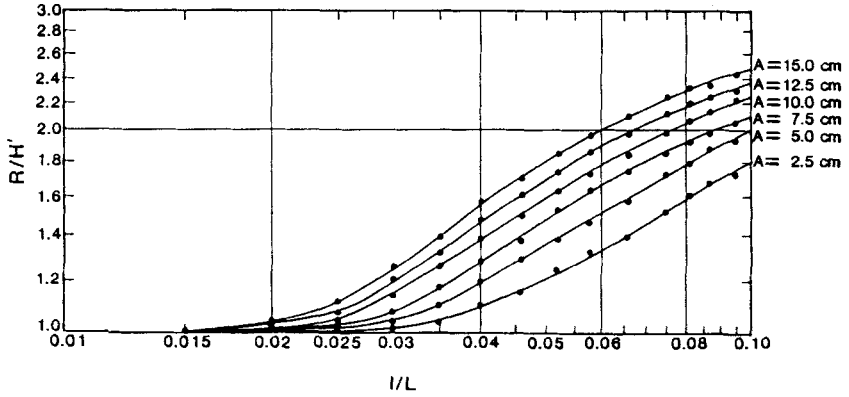

Figure 16. Claculated relationship between R/H' and l/L

The initial conditions of velocity and water elevation are assumed to be zero for all domains analysed. A selective lumping parameter $e=0{\cdot}9$ and a time increment $\Delta t=0{\cdot}05$ s are employed. The wave-forms from time $t=71$ to 99 s are shown in Figure 20.

5.3. Wave run-up analysis of a channel of wedge-shaped cross-section

As an example of two-dimensional analysis, a wave run-up analysis of a channel of wedge-shaped cross-section has been carried out. Figure 21(a) is the initial finite element idealization in the still water state. Figures 21(b)–21(d) are the cross-sections A–A′, B–B′ and C–C′ respectively. The wave height is 2 m and the wave period is 10 s on the boundary a–b.

The boundary conditions used are as follows:

$$v=0 \quad \text{on a–d and b–c,}$$

$$\eta=A\sin(2\pi/T)t \qquad \text{on a–b,} \tag{15a}$$

$$u=\eta\sqrt{[g/(h+\eta)]} \qquad \text{on a–b.} \tag{15b}$$

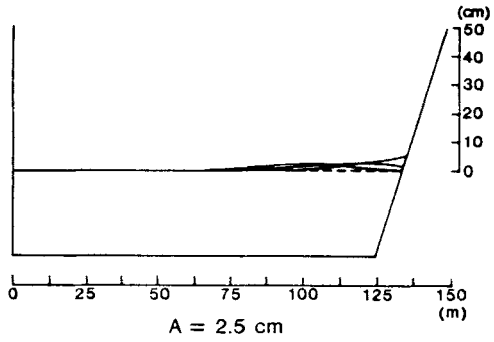

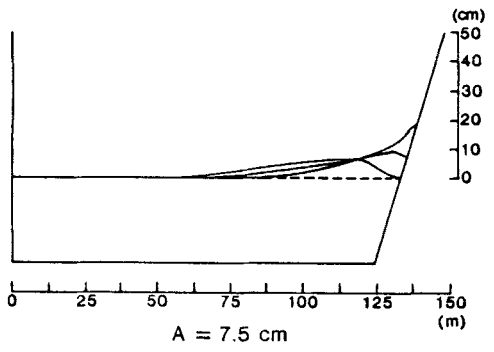

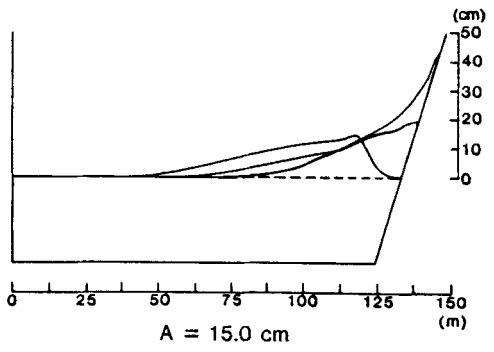

Figure 17. Wave profiles (wave period 60 s)

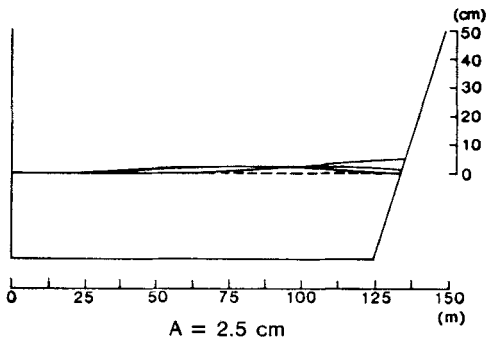

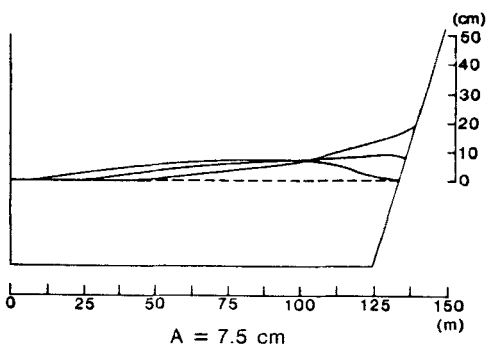

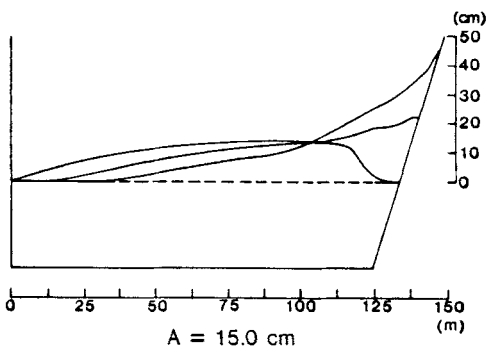

Figure 18. Wave profiles (wave period 130 s)

The initial conditions of velocity and water elevation are assumed to be zero for the domain analysed. A selective lumping parameter $e=0{\cdot}9$ and a time increment $\Delta t=0{\cdot}01$ s are employed.

Figures 22 and 24 show the cases where the wave is moving upwards and downwards respectively, while Figure 23 shows the intermediate case where upward and downward waves are interfering with each other. In Figures 22–24 parts (a)–(c) are the mesh configuration, velocity vector and water elevation respectively. From these figures the analysis presented in this paper is seen to be adaptable to channels of wedge-shaped cross section.

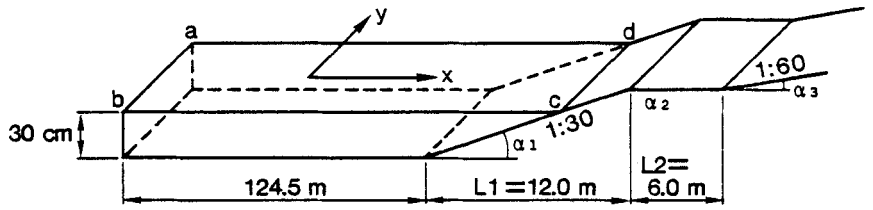

(a) Computational model

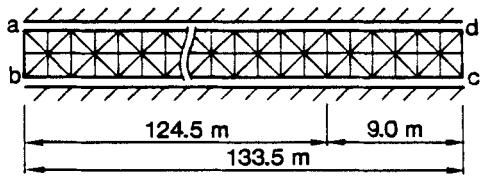

(b) Finite element idealization

Figure 19. Computational model and finite element idealization

5.4. Analysis of tsunami run-up caused by the 1983 Nihonkai-Chubu earthquake

The method has been applied to an actual tsunami run-up problem. The wave run-up of the tsunami caused by the 1983 Nihonkai-Chubu earthquake is analysed. The area to be analysed is the neighborhood of the estuary of the Mizusawa river (Akita Prefecture in Japan) where the highest run-up wave height was recorded.[36] The size of the domain to be analysed is an area 1200 m wide and 500 m long as shown in Figure 25. The finite element idealization and the topography of the land are also shown in this figure. The slope of the sea bottom is almost uniform at 1/100. Solid lines indicate the finite element idealization used for the computation of fluid and dotted lines that used for the interpolation of water depth. Line a–d is the shoreline. The lengths of finite elements are from 12·5 to 50 m.

The calculation is carried out by imposing the incident wave on the offshore boundary b–c. The wave imposed is of 6 m height and 600 s period. These conditions are obtained from the calculations in References 31, 33 and 34.

The boundary conditions used are as follows:

$$u=0 \qquad \text{on a–b and c–d,}$$

$$\eta=A\sin(2\pi/T)t \qquad \text{on b–c,} \tag{16a}$$

$$v=\eta\sqrt{[g/(h+\eta)]} \qquad \text{on b–c.} \tag{16b}$$

The initial conditions of velocity and water elevation are assumed to zero in the domain analysed. A selective lumping parameter $e=0{\cdot}9$ and a time increment $\Delta t=0{\cdot}3$ s are used for the computation.

Figures 26(a) and 26(b) show the computed results at $t=270$ and 300 s respectively. At $t=270$ s the tsunami run-up wave on the left and right sides of the domain arrives at the highest position whereas that in the middle part is still moving upwards. At $t=300$ s the wave on the left and right sides is moving downwards and that in the middle part arrives at the highest position. The run-up wave is influenced considerably by the topography of the land. Figure 27 shows the comparison

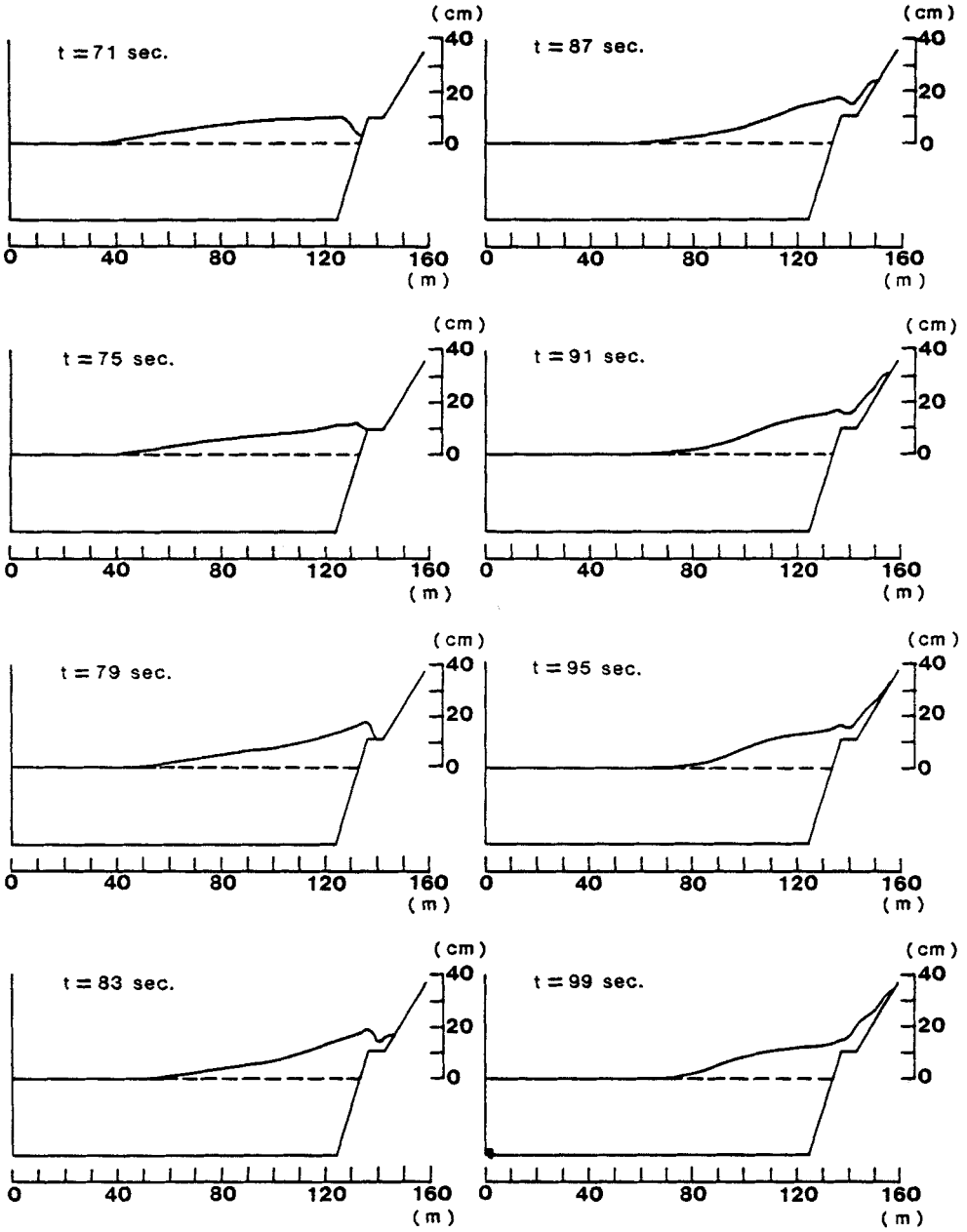

Figure 20. Wave configurations from time $t = 71$ to 99 s

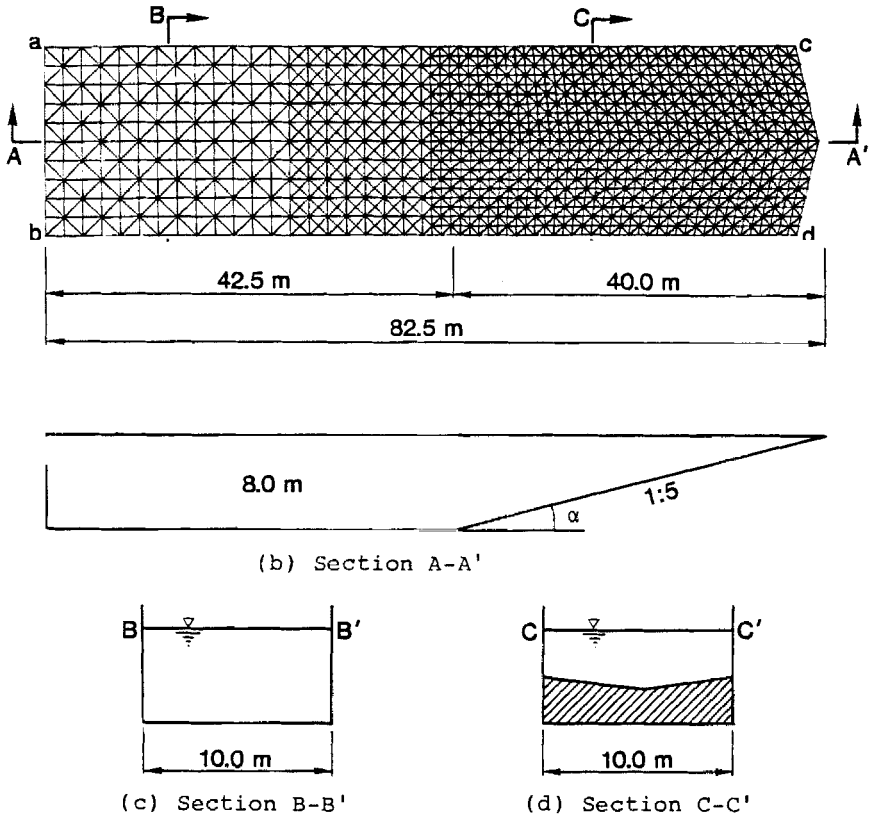

Figure 21. Computational model and finite element idealization

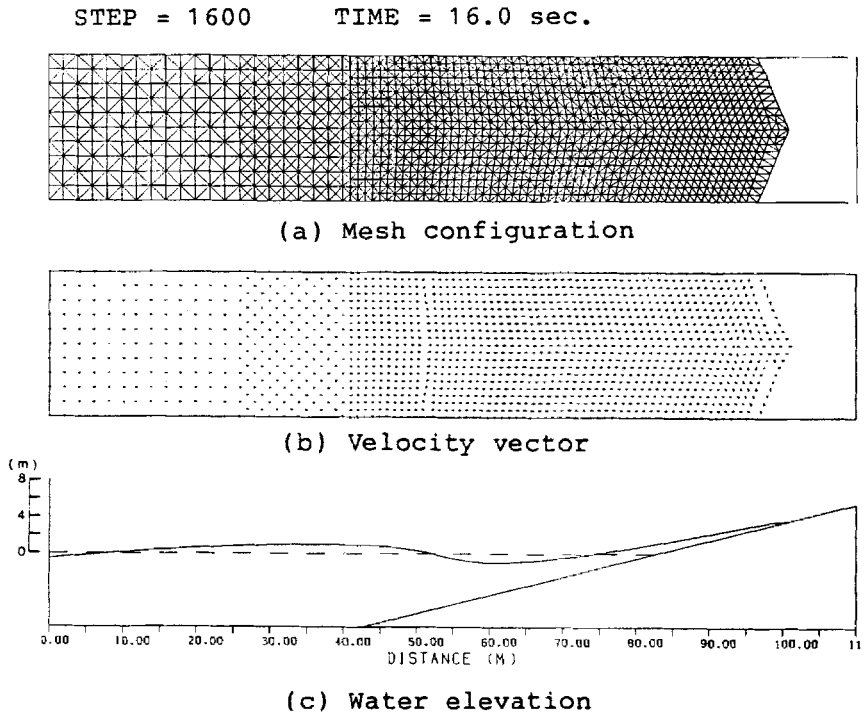

Figure 22. Computed results for wave moving upwards

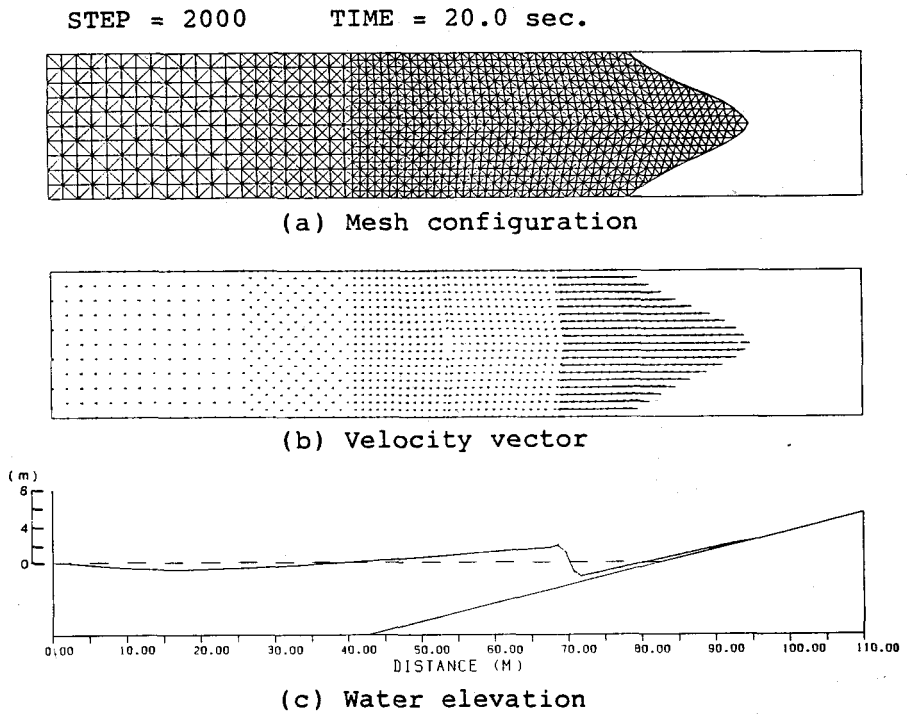

Figure 23. Computed results for upward and downward waves interfering

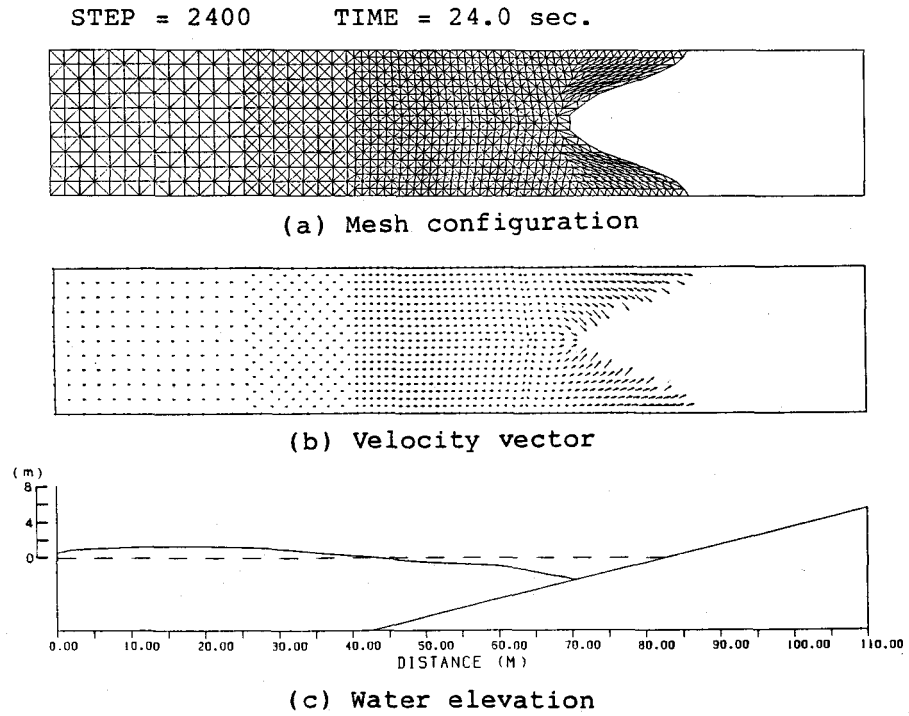

Figure 24. Computed results for wave moving downwards

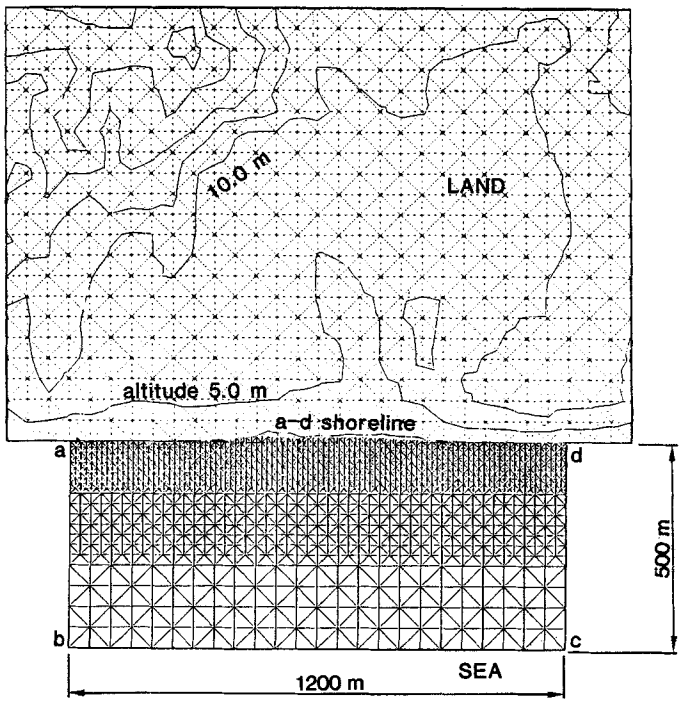

Figure 25. Finite element idealization and topography of the land

between the recorded and computed flood area. The flood area is an envelope of the highest positions of the run-up wave. The agreement is not as good as in the case of one- dimensional channel experiments. The reason seems to be the insufficiency of detailed information on both the topography of the land and the incident tsunami wave imposed on the offshore boundary. If more detailed information were used, better agreement could be obtained.

6. CONCLUSIONS

This paper presents a new finite element method for the analysis of the wave run-up problem. The conclusions derived are as follows.

(1) It is easy to compute the moving boundary problem by this method because the finite element region which is varying with time coincides with the region occupied by fluid.
(2) The numerical results by this method agree well with the experimental results for a channel of uniform slope.
(3) It is shown by numerical examples that the automatic mesh generation technique is effective for the two-dimensional analysis of moving boundary problems.
(4) This method is adaptable to the analysis of wave run-up problems with complicated beach topography, e.g. tsunami run-up analysis.
(5) In the case of an actual tsunami run-up analysis, detailed information about the land topography and incident wave is necessary.

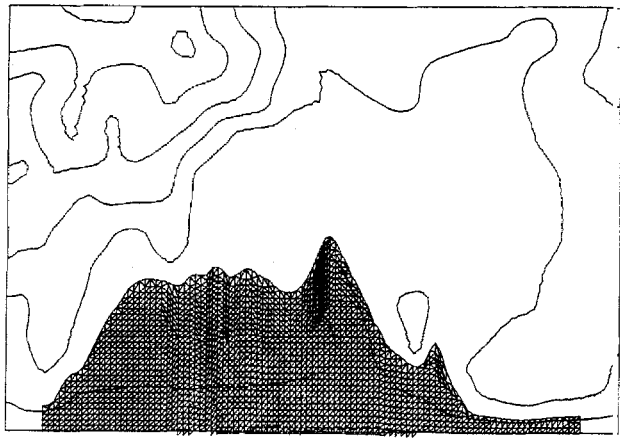

(a) t=270 sec.

(b) t=300 sec.

Figure 26. Computed results at $t = 270$ and 300 s

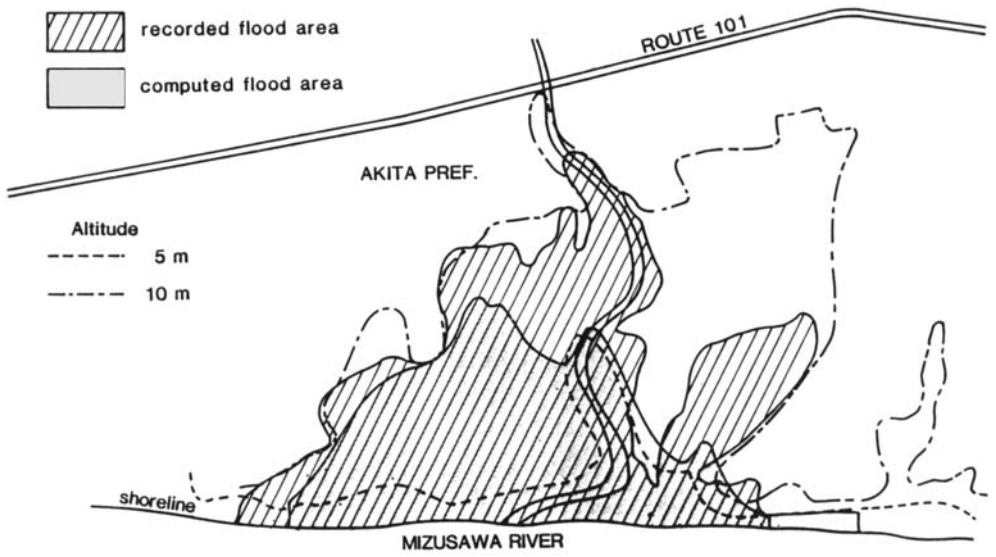

Figure 27. Comparison of the recorded flood area with the calculated result

REFERENCES

1. A. T. Ippen and G. Kulin, 'The shoaling and breaking of the solitary wave', *Proc. 5th Conf. on Coastal Engineering*, ASCE, 1954, pp. 27–47 (1954).
2. K. Kaplan, 'Generalized laboratory study of tsunami run-up', *Tech. Memo. No. 60*, BEB, Corps of Engineers, 1955.
3. T. Kishi, 'Transformation, breaking and run-up of a long wave of finite height', *Proc. 8th Conf. on Coastal Engineering*, ASCE, 1962, pp. 60–76 (1962).
4. Y. Iwagaki, M. Inoue and K. Obori, 'Experimental study on the mechanism of wave run up on slopes', *Proc. 13th Conf. on Coastal Engineering in Japan*, 1966, pp. 199–205 (in Japanese).
5. Y. Iwagaki, 'Hyperbolic waves and their shoaling', *Proc. 11th Conf. on Coastal Engineering*, ASCE, 1968, pp. 124–144 (1968).
6. F. E. Camfield and R. L. Street, 'Shoaling of solitary waves on small slopes', *Proc. ASCE*, **94** (WW1), 1–22 (1969).
7. T. Nakamura and H. Togashi, 'Reexamination of the experimental equations of run up of long wave', *Rep. Fac. Eng. Nagasaki Univ.*, **5**, 83–88 (1974).
8. T. Nakamura and H. Togashi, 'Reexamination of the experimental equations of run up of long wave (II)', *Rep. Fac. Eng. Nagasaki Univ.*, **7**, 73–78 (1976).
9. H. Togashi and T. Nakamura, 'Experimental research on run-up height of tsunami', *Proc. 22nd Conf. on Coastal Engineering in Japan*, JSCE, 1975, pp. 371–375 (in Japanese) (1975).
10. G. F. Carrier and H. P. Greenspan, 'Water waves of finite amplitude on a sloping beach', *J. Fluid Mech.*, **4**, 97–109 (1958).
11. H. P. Greenspan, 'On the breaking of water waves of finite amplitude on a sloping beach', *J. Fluid Mech.*, **4**, 330–334 (1958).
12. N. Shuto and K. Matsumura, 'Long waves—run-up height of long waves on an uniformly sloping beach', *Proc. 12th Conf. on Coastal Engineering in Japan*, JSCE, 1965, pp. 176–179 (in Japanese) (1965).
13. N. Shuto, 'Run-up of long waves on a sloping beach', *Coastal Eng. Jpn.*, **10**, 23–38 (1967).
14. N. Shuto, 'Standing wave in front of a sloping dike', *Coastal Eng. Jpn.*, **15**, 13–23 (1972).
15. R. Grimshaw, 'The solitary wave in water of variable depth', *J. Fluid Mech.*, **42**, 639–656 (1970).
16. J. C. Freeman and B. L. Méhauté, 'Wave breakers on a beach and surges on a dry bed', *Proc. ASCE*, **90** (HY2), 187–216 (1964).
17. M. Amein, 'Bore inception and propagation by the nonlinear wave theory', *Proc. 9th Conf. on Coastal Engineering*, ASCE, 1964, pp. 70–81 (1964).
18. D. H. Peregrine, 'Long waves on a beach', *J. Fluid Mech.*, **27**, 815–827 (1967).
19. D. H. Peregrine, 'Calculation of the development of an undular bore', *J. Fluid Mech.*, **25**, 321–330 (1966).
20. H. B.. Keller, D. A. Levine and G. B. Whitham, 'Motion of a bore over a sloping beach', *J. Fluid Mech.*, **7**, 302–316 (1960).

21. R. L. Street, R. K. C. Chan and J. E. Fromm, 'The numerical simulation of long water waves: progress on two fronts', *Proc. Int. Symp. on Tsunami and Tsunami Research*, 1969, pp. 453–473.
22. F. H. Harlow and J. E. Welch, 'Numerical calculation of time dependent viscous incompressible flow of fluid with free surface', *Phys. Fluids*, **8**, 2182–2189 (1965).
23. I. Aida, 'Numerical experiments for inundation of tsunamis Susaki and Usa, in Kochi Prefecture', *Bull. Earthquake Res. Inst. Univ. Tokyo*, **52**, 441–460 (1977).
24. I. Aida, 'Numerical experiments of tsunamis inundating Owase city, Central Japan', *Bull. Earthquake Res. Inst. Univ. Tokyo*, **57**, 337–350 (1982).
25. K. L. Heitner and G. W. Housner, 'Numerical model for tsunami run-up', *Proc. ASCE*, **96** (WW3), 701–719 (1970).
26. T. C. Gopalakrishnan and C. C. Tung, 'Numerical analysis of a moving boundary problem in coastal hydrodynamics', *Int. j. numer. methods fluids*, **3**, 179–200 (1983).
27. T. C. Gopalakrishnan and C. C. Tung, 'Run-up of non-breaking waves—a finite-element approach', *Coastal Eng.*, **4**, 3–22 (1980).
28. M. Kawahara, H. Hirano, K. Tsubota and K. Inagaki, 'Selective lumping finite element method for shallow water flow', *Int. j. numer. methods fluids*, **2**, 89–112 (1982).
29. M. Kawahara and H. Hirano, 'Two step explicit finite element method for high Reynolds number viscous fluid flow', *Proc. Jpn. Soc. Civil Eng.*, (329), 127–140 (1983).
30. M. Kawahara and H. Hirano, 'A finite element method for high Reynolds number viscous fluid flow using two step explicit scheme', *Int. j. numer. methods fluids*, **3**, 137–163 (1983).
31. T. Okamoto, K. Kidera and M. Kawahara, 'Predictive analysis of tsunami by selective lumping finite element method', *Proc. Sixth Int. Symp. on Finite Element Methods in Flow Problems, INRIA*, 1986, pp. 519–523 (1986).
32. N. Ioki and M. Kawahara, 'Selective lumping finite element method for analysis of wave run-up', *Int. Conf. Com. Mech.*, **2**, 157–162 (1986).
33. I. Aida, 'A source model of the tsunami accompanying the 1983 Nihonkai-Chubu earthquake', *Bull. Earthquake Res. Inst. Univ. Tokyo*, **59**, 93–104 (1984).
34. I. Aida, 'Tsunami magnitude and source area of Nihonkai-Chubu (the Japan sea) earthquake in 1983', *Bull. Earthquake Res. Inst. Univ. Tokyo*, **58**, 723–734 (1983).
35. K. Kashiyama and M. Kawahara, 'Interpolation method for preparation of input data of water depth in finite element analysis of shallow water flow', *Eng. Comput.*, **2**, 265–270 (1985).
36. 'The 1983 Nihonkai-Chubu earthquake—disaster report of public institutions', Akita Prefecture Civil Engineering Department, 1984.